The Astrophysical Journal Letters, 971:L30 (10pp), 2024 August 20 https://doi.org/10.3847/2041-8213/ad6864

GRB 211211A: The Case for an Engine-powered over *r*-process-powered Blue Kilonova

Hamid Hamidani[1], Masaomi Tanaka[1], Shigeo S. Kimura[1,2], Gavin P. Lamb[3], and Kyohei Kawaguchi[4,5]
[1] Astronomical Institute, Graduate School of Science, Tohoku University, Sendai 980-8578, Japan; hhamidani@astr.tohoku.ac.jp
[2] Frontier Research Institute for Interdisciplinary Sciences, Tohoku University, Sendai 980-8578, Japan
[3] Astrophysics Research Institute, Liverpool John Moores University, Liverpool Science Park IC2, 146 Brownlow Hill, Liverpool, L3 5RF, UK
[4] Max Planck Institute for Gravitational Physics (Albert Einstein Institute), Am Mühlenberg 1, Potsdam-Golm, 14476, Germany
[5] Center of Gravitational Physics and Quantum Information, Yukawa Institute for Theoretical Physics, Kyoto University, Kyoto, 606-8502, Japan
Received 2024 June 28; revised 2024 July 17; accepted 2024 July 28; published 2024 August 12

Abstract

The recent gamma-ray burst (GRB) GRB 211211A provides the earliest (∼5 hr) data of a kilonova (KN) event, displaying bright ($\sim 10^{42}$ erg s^{-1}) and blue early emission. Previously, this KN was explained using simplistic multicomponent fitting methods. Here, in order to understand the physical origin of the KN emission in GRB 211211A, we employ an analytic multizone model for *r*-process-powered KNe. We find that *r*-process-powered KN models alone cannot explain the fast temporal evolution and the spectral energy distribution (SED) of the observed emission. Specifically, (i) *r*-process models require high ejecta mass to match early luminosity, which overpredicts late-time emission, while (ii) red KN models that reproduce late emission underpredict early luminosity. We propose an alternative scenario involving early contributions from the GRB central engine via a late low-power jet, consistent with plateau emission in short GRBs and GeV emission detected by Fermi-LAT at $\sim 10^4$ s after GRB 211211A. Such late central engine activity, with an energy budget of ∼a few percent of that of the prompt jet, combined with a single red KN ejecta component, can naturally explain the light curve and SED of the observed emission, with the late-jet–ejecta interaction reproducing the early blue emission and *r*-process heating reproducing the late red emission. This supports claims that late low-power engine activity after prompt emission may be common. We encourage early follow-up observations of future nearby GRBs and compact binary merger events to reveal more about the central engine of GRBs and *r*-process events.

Unified Astronomy Thesaurus concepts: Gamma-ray bursts (629); R-process (1324); Neutron stars (1108); Relativistic jets (1390); Hydrodynamics (1963); Gravitational waves (678)

1. Introduction

Traditionally, gamma-ray bursts (GRBs) are classified into two classes based on their duration (T_{90}): long (LGRB; $T_{90} > 2$ s) and short (SGRB; $T_{90} < 2$ s) (Kouveliotou et al. 1993). On one hand, LGRBs are explained by the collapse of massive stars (collapsar model; MacFadyen & Woosley 1999), and in fact, most nearby LGRBs (with a few exceptions: GRB 060614, GRB 060505, etc.) are associated with bright supernova (SN) explosions confirming this scenario (Iwamoto et al. 1998; Stanek et al. 2003). On the other hand, SGRBs have theoretically been associated with binary neutron star (BNS; also black hole–neutron star, BH–NS) mergers (Goodman 1986; Paczynski 1986). This scenario is consistent with observations that show spatial offsets between SGRB locations and their candidate host galaxies (Fong et al. 2010, 2022; Nugent et al. 2022; O'Connor et al. 2022).

Moreover, BNS mergers are a site of *r*-process nucleosynthesis whose radioactivity powers an optical-infrared transient referred to as a "kilonova/macronova" (hereafter KN; Li & Paczyński 1998; Kulkarni 2005; Metzger et al. 2010). This was confirmed with the gravitational-wave (GW) and electromagnetic observations of GW170817, associating a BNS merger event with an SGRB (GRB 170817A) and with the KN transient AT 2017gfo (e.g., Abbott et al. 2017a, 2017b; Drout et al. 2017; Kasliwal et al. 2017; Tanaka et al. 2017).

Observations of GRB 211211A show a long main peak (∼13 s according to Fermi-GBM), followed by a softer and smoother extended emission (∼55 s long, Fermi-GBM; Rastinejad et al. 2022; Troja et al. 2022; Yang et al. 2022; Veres et al. 2023). A candidate host galaxy was identified, allowing for redshift ($z = 0.0762$) and distance ($d_L = 346$ Mpc) measurements (Rastinejad et al. 2022; Troja et al. 2022). As a bright nearby GRB, GRB 211211A was the target of many follow-up observations. However, although according to the traditional classification scheme, GRB 211211A is an LGRB, no sign of an SN could be found, while a clear KN transient was identified (Rastinejad et al. 2022; Troja et al. 2022). This suggests that GRB 211211A originated from a BNS/BH–NS merger event, and that SGRBs' engine activity can last longer than the nominal 2 s duration limit (see Figure 2 in Kisaka & Ioka 2015; Gao et al. 2022; Gottlieb et al. 2023; also see Gillanders et al. 2023; Levan et al. 2024; Yang et al. 2024 for the similar event GRB 230307A).

Thanks to its nearby location, the KN that followed GRB 211211A was observed at times earlier than any event before (Rastinejad et al. 2022; Troja et al. 2022). These observations revealed a bright early blue KN ($\sim 3 \times 10^{42}$ erg s^{-1} at ∼5 hr; Troja et al. 2022). The origin of this blue KN (also in the GW170817/AT 2017gfo event; Drout et al. 2017; Kasliwal et al. 2017) is not well understood, considering that KNe are expected to peak in optical-infrared bands, as they contain substantial fractions of heavy elements (i.e., lanthanides, with high opacities). Through the fitting of photometric data, it has been shown that the KN is well explained by two or three ejecta components (red, blue, and purple) with given masses, opacities, and velocities (Rastinejad et al. 2022).

However, these methods (e.g., Villar et al. 2017) are based on one-zone models (Arnett 1982). Additionally, parameter fitting results are often at odds with first-principle numerical relativity simulations (see Shibata et al. 2017; Fujibayashi et al. 2018; Kawaguchi et al. 2018; Siegel 2019). Therefore, it is crucial to investigate the origin of the blue KN emission using more sophisticated models.

Another key observation related to GRB 211211A is the detection of high-energy ($\sim$0.1−1 GeV) photon emission by Fermi-LAT $\sim 10^4$ s after the prompt emission (Mei et al. 2022; Zhang et al. 2022). This is the first time that late-time GeV emission from a supposed BNS merger event has been detected with high significance at $>5\sigma$ (GRB 160821B is another similar event where sub-TeV emission was detected by MAGIC, although less significantly at $\sim 3\sigma$; Lamb et al. 2019; Acciari et al. 2021; Zhang et al. 2021). The GeV emission was explained by KN photons interacting (via inverse Compton scattering) with a low-power jet powered by the central engine long after the prompt phase (Mei et al. 2022). Zhang et al. (2022) suggested that the afterglow model could explain this emission; however, this requires extreme jet parameters ($E_{\rm k,iso} \sim 10^{53}$ erg and $\theta_j \sim 1°$).

The idea that the GRB engine stays active long after the prompt emission is not new;[6] observations have consistently shown that $\sim 10^2$−10^4 s after the prompt emission, bright X-ray emission that cannot be explained by the standard afterglow model is emitted (see Barthelmy et al. 2005b; Gompertz et al. 2013; Kisaka et al. 2017; Kagawa et al. 2019; etc.). These late phases are referred to as "extended" (with $L_{\rm X} \sim 10^{48}$ erg s^{-1} for $\sim 10^2$ s) or "plateau" (with $L_{\rm X} \sim 10^{46}$ erg s^{-1} for $\sim 10^4$ s) phases and are typically associated with late engine activity (Ioka et al. 2005; Kisaka & Ioka 2015; Gottlieb et al. 2023; etc.). These late phases of engine activity might be ubiquitous in SGRBs (Kisaka et al. 2017).[7]

In an effort to understand the origin of KN transients, we revisit GRB 211211A, which provides the earliest data of a KN to date. We investigate the source of the bright early blue KN emission via analytic modeling and test the hypothesis that this blue emission is *r*-process-powered. Additionally, we explore the impact of a late low-power (i.e., plateau) jet interacting with the merger ejecta on the KN emission.

This Letter is organized as follows. In Section 2, we present our physical model for *r*-process-powered KNe. In Section 3, we present our results and explain the limitations of the *r*-process-powered KN scenario. An alternative scenario of central-engine-powered KNe is presented in Section 4. Finally, a discussion and conclusion are presented in Section 5. Details related to GRB 211211A's data can be found in the Appendix.

2. Method

2.1. R-process-powered KN Model

We consider the same KN model as in Hamidani et al. (2024; see their Appendix E), with additional improvements. The main approximations of the model are as follows.

1. The ejecta is expanding homologously with $\beta_{\rm m}$ and β_0 as the maximum and minimum velocities (in units of c), respectively.
2. The density profile of the ejecta is approximated to a single power law with n as its power-law index:
$$\rho \propto \beta^{-n}. \quad (1)$$
This is significantly more realistic than the widely used KN models (e.g., see Section 3 in Villar et al. 2017), as the time evolution of optical depth, photospheric radius, luminosity, and temperature depend on the spatial distribution of density.
3. The time evolution of *r*-process energy deposition per mass ($\dot{\varepsilon}$) is approximated to a power-law function,
$$\dot{\varepsilon} = \dot{\varepsilon}_0 \left(\frac{t}{1\ {\rm day}} \right)^{-k}, \quad (2)$$
with $k = 1.3$ and $\dot{\varepsilon}_0 = 2 \times 10^{10}$ erg g^{-1} s^{-1} (i.e., $\dot{\varepsilon}_0 \sim$ 1 MeV nuc^{-1} s^{-1} at $t = 0.1$ s; Wanajo et al. 2014; Ishizaki et al. 2021).
4. At early times (the first few days), *r*-process energy deposition is assumed to be dominated by beta decay (Wanajo et al. 2014; Kasen & Barnes 2019).[8] Hence, we adopt an analytic time-dependent thermalization efficiency term $f_{\rm tot}(t)$ (Barnes et al. 2016; Hotokezaka et al. 2016) following the analytic model in Kasen & Barnes (2019; see their Equation (51)). In reality, $f_{\rm tot}(t)$ should also have spatial dependency, but here, for simplicity, we consider a one-zone prescription.
5. A sharp diffusion shell at
$$\tau = c/(v_{\rm m} - v_{\rm d}) \quad (3)$$
is adopted, where $\beta_{\rm m} = v_{\rm m}/c$ and $\beta_{\rm d} = v_{\rm d}/c$ are the outer velocity of the ejecta and the velocity of the sharp diffusion shell, respectively (Nakar & Sari 2012; Kisaka et al. 2015; Hamidani & Ioka 2023a).
6. Gray opacity is adopted,
$$\kappa = {\rm Const.}, \quad (4)$$
with κ values taken from realistic radiative transfer simulation results (see Banerjee et al. 2024).
7. In the first few days, the KN emission is approximated to a blackbody (Kisaka et al. 2015; Waxman et al. 2018).

For a given shell in the ejecta with a velocity β, density, optical depth, and thermal energy density can be found as a function of time. Then, with the photon diffusion criteria, emission can be found analytically as a function of time. Therefore, for a given set of the following parameters, KN emission (light curve and spectral energy distribution, SED) can be found analytically: ejecta mass ($M_{\rm e}$), power-law index of the density profile of the ejecta (n), maximum ejecta velocity ($\beta_{\rm m}$), minimum ejecta velocity (β_0), and gray opacity (κ).

There are two distinct terms that contribute to the KN emission, as follows (Equation (E3) in Hamidani et al. 2024):
$$L_{\rm KN}(t) = L_{\rm KN}(<\beta_{\rm d}, t) + L_{\rm KN}(\geqslant\beta_{\rm d}, t), \quad (5)$$
where t is time ($t \approx t_{\rm obs}$) and $\beta_{\rm d}$ is the velocity of the diffusion shell. The first term ($L_{\rm KN}(<\beta_{\rm d}, t)$) is emission due to leaking of trapped thermal (or internal) energy as the diffusion shell moves inward (in a Lagrangian coordinate) through the

[6] There is a similar argument for LGRBs based on observations of X-ray flares (Burrows et al. 2005; Nousek et al. 2006).

[7] For GW170817/GRB 170817A, these late phases could not be confirmed due to the off-axis line of sight and the earliest follow-up observations being too late (Evans et al. 2017).

[8] This is a conservative consideration, as it gives a faster time evolution for $f_{\rm tot}$ (without alpha and fission contributions) and considers our aim of exploring alternative scenarios that explain the fast time evolution in the light curve of the KN associated with GRB 211211A.

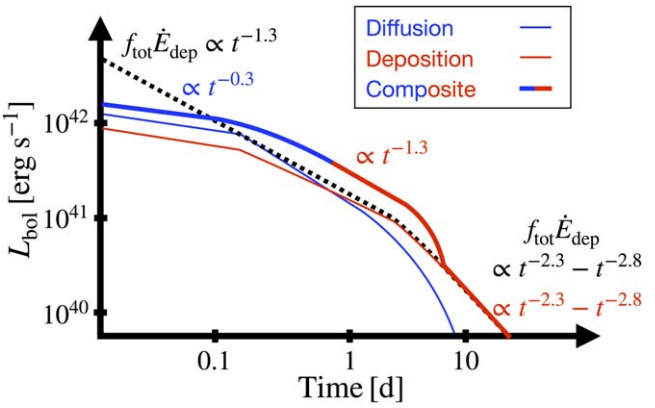

Figure 1. Time evolution of *r*-process-powered KN light curve. The early blue KN emission (thick blue line) is $\propto t^{-0.3}$, as it is mostly powered by diffusion emission (thin blue line; first term in Equation (5)). After a transitional phase, later emission (thick red line) follows the deposition rate of thermal energy through the *r*-process (thin red line in the optically thin part and dashed line in the whole ejecta) as $\propto t^{-1.3}$ (second term in Equation (5)) and asymptotically as $\propto t^{-2.3} - t^{-2.8}$ (for a similar figure, see Figure 4 in Kasen & Barnes 2019; also see Waxman et al. 2019; Hotokezaka & Nakar 2020).

optically thick part of the ejecta; we refer to it as the "diffusion" term. The second term ($L_{\rm KN}(\geqslant \beta_{\rm d},\ t)$) is emission due to instantaneous deposition of thermal energy (via *r*-process heating) in the optically thin part of the ejecta; we refer to it as the "deposition" term.

As shown in Figure 1, at early times (typically <1 day), the diffusion part is largely dominant; however, at later times, as the majority of the ejecta mass is exposed in the optically thin outer part, the second term takes over.

The time evolution of the term that represents the trapped thermal energy $E_{\rm i}(<\beta_{\rm d},\ t)$ at shells moving with velocities slower than $\beta_{\rm d}$ can be found by considering energy deposition by *r*-process and adiabatic cooling, giving $\partial E_{\rm i}(<\beta_{\rm d},\ t)/\partial t = -E_{\rm i}(<\beta_{\rm d},\ t)/t + f_{\rm tot}(t)\dot{E}_{\rm dep}(<\beta_{\rm d},\ t)$. Hence,

$$E_{\rm i}(<\beta_{\rm d},\ t) = \frac{1}{t}\int_0^t f_{\rm tot}(t)\dot{E}_{\rm tot}(<\beta_{\rm d},\ t)tdt \propto t^{1-k} f_{\rm tot}(t) M_{\rm e}(<\beta_{\rm d},\ t), \quad (6)$$

where $\dot{E}_{\rm dep}(<\beta_{\rm d},\ t) = M_{\rm e}(<\beta_{\rm d},\ t)\dot{\varepsilon}_0(t/1\ {\rm day})^{-k}$ is the *r*-process energy deposition in all shells slower than $\beta_{\rm d}$ with a mass $M_{\rm e}(<\beta_{\rm d},\ t)$.

At early times, a key approximation is that $\beta_{\rm d} \sim \beta_{\rm m}$, and hence $\rho(\beta_{\rm d},\ t) \sim \rho(\beta_{\rm m},\ t)$ (see Section 3.1 in Kisaka et al. 2015). From the condition of a sharp diffusion shell (Equation (3)), $1/(\beta_{\rm m} - \beta_{\rm d}) \propto \rho(\beta_{\rm m},\ t)t(\beta_{\rm m} - \beta_{\rm d})$, and the diffusion velocity moves inward through the ejecta so that $\beta_{\rm m} - \beta_{\rm d} \propto t$ [as $\rho(\beta_{\rm m},\ t) \propto t^{-3}$]. Consequently, during a time interval Δt, $(\beta_{\rm m} - \beta_{\rm d}) \propto \Delta t$, and the newly exposed mass $\Delta M_{\rm e}(<\beta_{\rm d},\ t) = \rho(\beta_{\rm m},\ t)\Delta V \propto \Delta t$. Hence, $\Delta M_{\rm e}(<\beta_{\rm d},\ t)/\Delta t \sim$ Const. In other words, at early times, the diffusion shell moves constantly in the mass coordinate (see Kisaka et al. 2015; also see Appendix E in Hamidani et al. 2024). Also, at early times, $f_{\rm tot}(t) \equiv f_{\rm tot} \sim 0.7$, as the density is high and most radioactive energy deposition is thermalized (except neutrinos). Therefore, at early times, the evolution of the KN luminosity $L_{\rm KN}(t) \sim L_{\rm KN}(<\beta_{\rm d},\ t) \sim \Delta E_{\rm i}/\Delta t$ can be found as (using Equations (5) and (6))

$$L_{\rm KN}(t) \propto t^{1-k} \propto t^{-0.3} \qquad \text{(early times)}. \quad (7)$$

Hence, as shown in Figure 1, at early times, the amount of trapped thermal energy to be released is expected to follow $\propto t^{-0.3}$. It should be stressed that this time dependency is independent of the parameters of the ejecta (such as n). This is consistent with Kisaka et al. 2015 (see their Equation (19) and Figure 3).

The time evolution of the second term simply follows the deposition rate of thermal energy through the *r*-process (initially as $\propto t^{-k}$). Early on, most radioactive energy is thermalized (except neutrinos, which account for ∼30% of the energy deposition, i.e., $f_{\rm tot} \sim 0.7$; see Wanajo et al. 2014; Barnes et al. 2016; Hotokezaka et al. 2016; Rosswog et al. 2017; Kasen & Barnes 2019; etc.). At much later times, as density decreases, $f_{\rm tot}$ drops as radioactive particles are less efficiently thermalized; hence, the thermal energy deposition rate eventually enters its asymptotic phase and follows a steeper decline in the range $\propto t^{-2.3}$ (Kasen & Barnes 2019) to $\propto t^{-2.8}$ (Waxman et al. 2019; Hotokezaka & Nakar 2020).

2.2. Application to GRB 211211A

We aim to investigate the origin of the KN emission associated with GRB 211211A and whether it can be entirely explained by *r*-process-powered KN emission (Rastinejad et al. 2022; Troja et al. 2022). We employ our analytical *r*-process KN model (see Section 2.1; see also Appendix E in Hamidani et al. 2024 for a full description). First, we search for a combination of two KN models (i.e., two ejecta components) capable of explaining the SED and the bolometric data: a blue KN model with low opacity (to explain the early blue emission) and a red KN model with high opacity (to explain the late red emission). We proceed as follows: first, we carry out a parameter search to find models capable of explaining the early time data, then we search for a complementary red KN model that explains the rest of the data (late-time data in particular).

The main parameters for each KN model are $M_{\rm e}$ and κ, as the KN emission depends strongly on them. Eleven values of $M_{\rm e}$ spread linearly in the interval $0.01-0.05\ M_\odot$, and 11 values of κ spread logarithmically in the interval $10^{-1}-10\ {\rm cm^2\ g^{-1}}$ (the range of values is motivated by the results of radiative transfer simulations with realistic atomic data in Banerjee et al. 2024). β_0 is taken as 0.05 as suggested by postmerger mass ejection and GW170817 results (see Fujibayashi et al. 2018; Waxman et al. 2018). We take $\beta_{\rm m} = 0.4$ (also $\beta_{\rm m} = 0.3$, although the results are similar). Finally, we take $n = 2$ as expected from postmerger mass ejecta (i.e., constant mass ejection $\dot{M}_{\rm e} \propto$ Const.; $n = 3.5$ has also been considered, but the results are similar).

We focus on two observational facts: (i) the early (5−10 hr) blue KN emission associated with GRB 211211A is quite luminous ($\sim 3-4 \times 10^{42}\ {\rm erg\ s^{-1}}$, see Table 1; Troja et al. 2022), and (ii) late observations at 4.4 days put an upper limit on the luminosity on the late red KN (in particular, an upper limit in the *R* band by Devasthal Optical Telescope (DOT); Troja et al. 2022). We search for combinations of KN models that can reproduce the early brightness and that do not overpredict (overshoot) the late red KN emission.

3. Results

3.1. The Light Curve

To reproduce the bright bolometric luminosity of the early blue KN emission in GRB 211211A (see Table 1 and Troja

et al. 2022), we search for viable *r*-process-powered KN models. Via an *r*-process-powered KN model, the bright early emission can be achieved by increasing the ratio M_e/κ; as the photon diffusion time is $\propto\sqrt{\kappa M_e}$, and *r*-process energy $E \propto M$, then $L \propto E/t \propto \sqrt{M_e/\kappa}$.

We use $n = 2$, which corresponds to a constant mass ejecta rate $\dot{M}_e \propto$ Const. As $L_{KN} \propto t^{-0.3}$ at early times regardless of n, n has a limited effect. The impact of the parameter β_m is also limited. This is because β_m has a physically limited range (as <1), and the temperature dependence on it in this range is not strong. Also, as the kinetic energy of the merger ejecta is $\propto\beta_m^2$, higher values ($\beta_m \sim 0.8$) are not allowed, as they imply very bright X-ray/radio emission from the merger ejecta, which has not been observed. The impact of β_0 is even weaker (as long as $\beta_0 \ll \beta_m$).

Hence, either a low κ or a high M_e parameter space is expected to explain the bright early KN emission. However, it should be stressed that a KN model that overpredicts the late red KN emission (at $\sim$4 days) should also be ruled out. There are two important properties of *r*-process-powered emission to recall: (i) *r*-process energy deposition is $\propto t^{-1.3}$, and early emission is dominated by diffusion of trapped thermal energy, which has a shallow luminosity evolution ($\propto t^{-0.3}$ at early times, see Equation (7); see Section 2.1 and Figure 1); and (ii) luminosity at late times scales to the ejecta mass ($\propto M_e$). Hence, on one hand, employing a large ejecta mass model to explain the bright early KN emission can potentially overpredict the observed late red KN emission. On the other hand, adopting a low opacity ($\kappa \sim 0.1\ \mathrm{cm^2\ g^{-1}}$) and a less massive ejecta mass ($\sim 0.02\ M_\odot$) could avoid the issue of overpredicting the late red KN emission; however, while this might reproduce the early bolometric luminosity, the emission would be shifted too far into bluer colors and would consequently underproduce (undershoot) the observed blue KN emission in the optical bands. Adopting higher opacities ($\kappa \sim 1\ \mathrm{cm^2\ g^{-1}}$) would avoid this problem but, again, at the expense of making the early bolometric luminosity (calculated using Equation (E5) in Appendix E of Hamidani et al. 2024) too faint to explain the early observations (5–10 hr epoch; similar effects can be seen in Figure 3 for $M_e \sim 0.04\ M_\odot$ and $\kappa \sim 0.1-10\ \mathrm{cm^2\ g^{-1}}$).

Figure 2 shows two light curves, the first from a blue KN model and the second from a red KN model, chosen to reproduce early and late observations, respectively. The tendency of the blue KN model to overpredict the observed late red emission, as well as the tendency of the late red KN model to underpredict the early blue emission, is apparent. The overall time evolution of the observed KN emission (early to late KN emission in GRB 211211A, as well as AT 2017gfo data) requiring a steeper power-law function (with an index between -1 and -1.3) than what is expected from the *r*-process at early times (see Equation (7) and Figure 1) is also apparent.

3.2. The SED

Figure 3 shows the SED for an afterglow and the *r*-process-powered KN models with varying opacities ($\kappa = 0.1\ \mathrm{cm^2\ g^{-1}}$, $\kappa = 1\ \mathrm{cm^2\ g^{-1}}$, and $\kappa = 10\ \mathrm{cm^2\ g^{-1}}$ in light gray, dark gray, and black, respectively) and $M_e = 0.04\ M_\odot$. As explained in Section 3.1, low opacity tends to shift the SED to higher frequencies. Consequently, an *r*-process-powered blue KN model with low opacity ($\kappa = 0.1\ \mathrm{cm^2\ g^{-1}}$), although it can give a bright enough early blue emission, is inconsistent with early

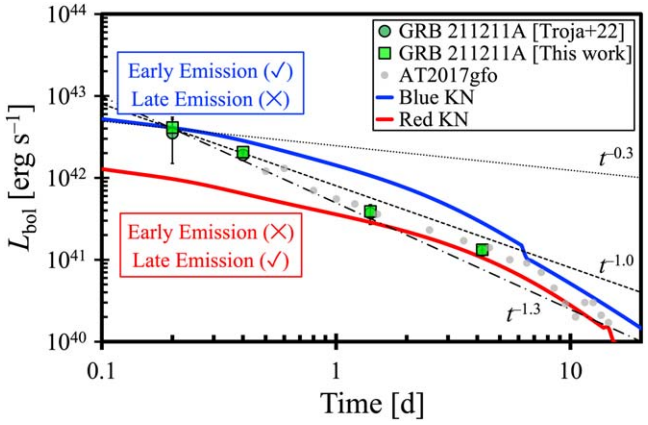

Figure 2. The bolometric luminosity for a blue KN model (blue line; $\kappa = 1\ \mathrm{cm^2\ g^{-1}}$ and $M_e = 0.05\ M_\odot$) that can explain the early KN emission in GRB 211211A (but overpredicts late KN emission) and a red KN model (red line; $\kappa = 10\ \mathrm{cm^2\ g^{-1}}$ and $M_e = 0.04\ M_\odot$) that can explain the late KN emission in GRB 211211A (but underpredicts late KN emission). The observed KN emission in GRB 211211A (dark gray squares for our fit and dark gray circles for Troja et al. 2022; see Table 1) and AT 2017gfo (gray circles; data from Waxman et al. 2018) are shown. Dotted, dashed, and dotted–dashed lines highlight time-evolving power-law functions with indices of -0.3, -1.0, and -1.3, respectively. This illustrates the difficulty of *r*-process-powered KN models in explaining the fast time evolution of the KN emission in GRB 211211A. Other parameters of the KN models are $\beta_0 = 0.05$, $\beta_m = 0.4$, and $n = 2$.

(and late) observations in terms of color (too blue). A moderate opacity of $\kappa = 1\ \mathrm{cm^2\ g^{-1}}$ requires a higher mass to match early observations (5–10 hr); however, such a high mass is incompatible with the late observations (1.4–4.2 days). In particular, such models overshoot the *R*-band upper limit at the 4.2 day epoch (more precisely at 4.4 days; see Table 1 in Troja et al. 2022). Hence, we find that it is challenging to explain the entire data set even with a combination of two *r*-process-powered KN models (blue KN and red KN models combined).

3.3. Constraining κ and M_e

We investigate whether there are other possible *r*-process-powered KN models, with different parameters, that could explain GRB 211211A's data set. Our main parameters are M_e and κ, set to take 11 values each in the range $0.01-0.05\ M_\odot$ and $0.1-10\ \mathrm{cm^2\ g^{-1}}$, respectively (see Section 2.2). The other parameters (β_m, β_0, and n) have been explored individually but were found to have limited effects.

Using our analytic model for *r*-process-powered KN, and as a test of the hypothesis that the blue KN is *r*-process-powered, we search for parameters where the KN associated with GRB 211211A can be explained in its entirety. First, we evaluate the bolometric luminosity and rule out the parameter space where the *r*-process-powered KN luminosity at early times (5–10 hr) is less than that of the KN in GRB 211211A (by more than 1σ; see Table 1). Then, we evaluate the observed νF_ν at late times ($\sim$1.4 days and $\sim$4.2 days) and rule out models that overshoot the data; in particular, the 3σ *R*-band upper limit (by DOT; Gupta et al. 2021) at 4.4 days poses a strict constraint (see Figure 3; also see Figure 2 in Troja et al. 2022). It should be noted that these two criteria are quite conservative.

As shown in Figure 4, we find no parameter space where both criteria are fulfilled. In summary, the observed blue KN emission after GRB 211211A is so bright that in order to

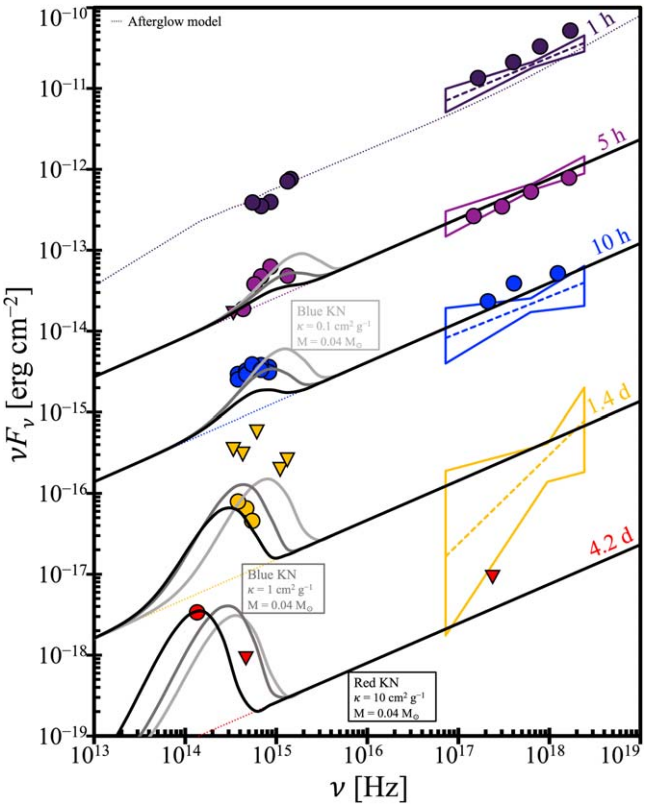

Figure 3. SED of GRB 211211A and its time evolution. Five epochs are shown: 1 hr (dark purple), 5 hr (purple), 10 hr (blue), 1.4 days (orange), and 4.2 days (red). Filled circles indicate detections, while triangles indicate upper limits. Central values for the X-ray's photon index (dashed lines) and the corresponding uncertainty (bow ties) are shown (see the Appendix). The afterglow model is shown at each epoch with a dotted line. Three *r*-process KN models are shown (using $z = 0.0762$): a low-opacity blue KN model ($\kappa = 0.1$ cm^2 g^{-1} and $M_e = 0.04\,M_\odot$; light gray), a moderate-opacity blue KN model ($\kappa = 1$ cm^2 g^{-1} and $M_e = 0.04\,M_\odot$; dark gray), and a red KN model ($\kappa = 10$ cm^2 g^{-1} and $M_e = 0.04\,M_\odot$; black). The inability of *r*-process-powered blue KN models to explain both early observations without overproducing late emission is apparent. Also, the inconsistency of the low-opacity model (light gray) with the color of early data is apparent. IR/optical/UV data points were taken from Rastinejad et al. (2022) and Troja et al. (2022), and X-ray data were taken from Troja et al. (2022). For clarity, the data are scaled at each epoch by the following factors: 10^0, $10^{-0.8}$, $10^{-1.6}$, $10^{-2.4}$, and $10^{-3.2}$ (same as in Troja et al. 2022). For a similar plot, see Figure 2 in Troja et al. (2022) and Extended Data Figure 2 in Rastinejad et al. (2022).

explain it via the *r*-process, a large mass (and/or low κ) is required, which (due to the shallowness of the early KN light curve; see Figure 1) ends up overpredicting (and contradicting) the late red KN emission data. This result suggests a different origin for the early blue KN emission in GRB 211211A, other than "*r*-process," such as the "central engine" (see Section 3).

4. The Alternative: Central-engine-powered KN

In Section 3, we found that the *r*-process-powered KN model has its limitations when explaining the early data in GRB 211211A; here we explore an alternative scenario.

It is important to highlight two important observational facts. First, observations of SGRBs (with a likely BNS merger origin) have consistently shown that, after the prompt phase, there is an extended/plateau phase (e.g., Barthelmy et al. 2005a; Norris & Bonnell 2006; Gompertz et al. 2013). This late phase is present in the majority of SGRBs (Kisaka et al. 2017), and it has been associated with late engine activity (Ioka et al. 2005).

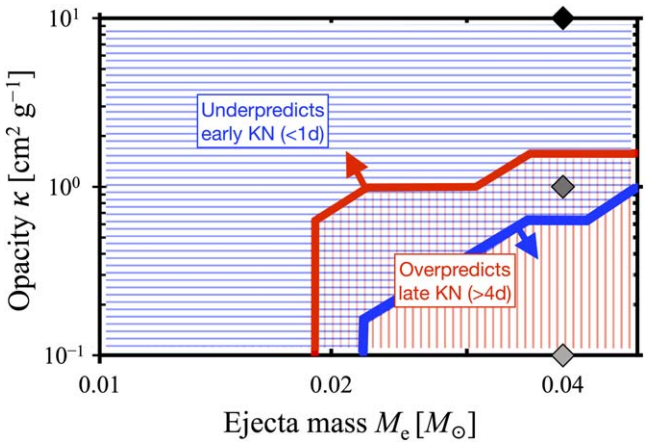

Figure 4. The ejecta mass (M_e) and opacity (κ) parameter space for *r*-process-powered KN models. The area constrained by the thick blue line (as indicated by the blue arrow) is where KN models are at least as bright as the early (5–10 hr) blue KN emission observed in GRB 211211A (within 1σ); blue stripes indicate the parameter space where this is not the case (ruled out). The area constrained by the thick red line (as indicated by the red arrow) is where the KN models do not overpredict the late-time red emission (1.4–4.2 days; see Figure 3); red stripes indicate the parameter space where this is not satisfied (ruled out). There is no eligible parameter space where both the early and late emission of the KN in GRB 211211A can be explained by a combination of two *r*-process-powered KN models. Diamond symbols indicate the three KN models shown in Figure 3. The other parameters are taken as $\beta_0 = 0.05$, $\beta_m = 0.4$, and $n = 2$ (found to have limited effects on the results).

Second, follow-up observations of GRB 211211A by Fermi-LAT detected GeV emission at $\sim 10^4$ s after the prompt emission (Mei et al. 2022). This late GeV emission has been explained with late central engine activity, launching a late (long-lasting) low-power jet that interacts with the KN (Kimura et al. 2019; Mei et al. 2022). Hence, these two observational facts support late engine activity launching a low-power jet in BNS merger systems, such as GRB 211211A and other SGRBs.

In an attempt to investigate the origin of the early blue KN emission in GRB 211211A and find an alternative to the *r*-process-powered KN scenario, we consider late central engine activity. Considering the timescale of the GeV emission ($\sim 10^4$ s after), we adopt a plateau-like, long-lasting ($\sim 10^4$ s), and low-power engine (i.e., $\sim$10% radiative efficiency). Since the typical luminosity of the plateau phase in X-rays is $\sim 10^{46}$ erg s^{-1} (Kisaka et al. 2017), we consider a jet with a total power of 10^{47} erg s^{-1}. The late jet opening angle is not well understood from observations, however, considering that SGRB-jet opening angles (measured via jet break) are typically $\sim 6^\circ$ (Rouco Escorial et al. 2023). We adopt a slightly larger, yet comparable, opening angle of $7^\circ.5$, as it has been suggested that the late jet takes a wider opening angle compared to the prompt jet (Lu & Quataert 2023).

In the central engine scenario, assuming the same ejecta as in the KN models, interaction of the central-engine-powered jet with the ejecta is considered. This jet–ejecta interaction produces a shock that converts kinetic energy into thermal energy in the form of a hot "cocoon" component surrounding the jet. As this thermal energy diffuses out of the ejecta, it produces the emission. This emission is calculated analytically in two steps as follows.

In the first step, we solve the jet propagation through the merger ejecta (via jump conditions) using the analytic model in Hamidani et al. (2020) and Hamidani & Ioka (2021); this

allows us to estimate the time it takes the jet to break out of the ejecta and estimate the amount of thermal energy produced via the jet–ejecta interaction in the form of a cocoon. For this, we use the above jet parameters ($L_{\rm iso,0}=10^{47}$ erg s^{-1} and $\theta_0=7.^\circ5$) and the ejecta parameters that correspond to the red KN model, $M_{\rm e}=0.04\,M_\odot$, $n=2$, and $\beta_{\rm m}=0.4$, with the exception that we use a much smaller inner velocity $\beta_0=\beta_{\rm m}/100$. The smaller inner velocity β_0 is motivated by the expected slower gravitationally bound component that is not relevant to the KN emission but is relevant to the jet propagation (at much earlier times). Note that the mass of this slower component is negligible (as $n=2$ and $M\propto\beta$), and the density profile here is the same as that in the red KN model.

In the second step, diffusion emission from the thermal energy produced in the jet–ejecta interaction is calculated analytically following Hamidani & Ioka (2023a, 2023b).[9] We focus on the diffusion emission from the cocoon trapped inside the ejecta ($<\beta_{\rm m}$), as this peaks at times relevant to the blue KN emission (see Appendix D in Hamidani et al. 2024). In addition, we estimate the ram pressure balance between the shocked ejecta (trapped cocoon) and the unshocked ejecta to determine the lateral spreading velocity ($\beta_\perp$) of the trapped cocoon; in the case where $\beta_\perp\gtrsim\beta_{\rm m}$, the trapped cocoon is considered to spread and reach a spherical asymptotic geometry. This was found to be the case for our central engine model.[10]

Diffusion emission from the thermal energy deposited by the jet–ejecta interaction gives an additional luminosity term ($L_{\rm CE}$) in addition to the two r-process terms in Equation (5) so that

$$L_{\rm tot}(t)=L_{\rm KN}(<\beta_{\rm d},\,t)+L_{\rm KN}(\geqslant\beta_{\rm d},\,t)+L_{\rm CE}(<\beta_{\rm d},\,t),\quad(8)$$

and $L_{\rm CE}$ can be found as (see Equation (12) in Hamidani et al. 2024; for more details, see their Appendix D)

$$L_{\rm CE}\approx 2.6\times10^{42}\ {\rm erg\ s^{-1}}\times\left(\frac{\theta_0}{7.^\circ5}\right)^2\left(\frac{L_{\rm iso,0}}{10^{47}\ {\rm erg\ s^{-1}}}\right)\left(\frac{t_{\rm b}}{4.7\times10^3\ {\rm s}}\right)\left(\frac{\kappa}{10\ {\rm cm^2\ g^{-1}}}\right)^{\frac{p-2}{2}}\left(\frac{M_{\rm e}}{0.04\,M_\odot}\right)^{\frac{p-2}{2}}\left(\frac{t_{\rm obs}}{5\ {\rm hr}}\right)^{-p},\quad(9)$$

where the index p takes values as $p\sim1$ (at $\sim$5–10 hr) to $p\sim2$ (at $\sim$1–4.2 days), which results in a steeper/faster time evolution than in the r-process model at early times (see Equation (7)). We use the exact same ejecta parameters as those of the red KN model (shown in Figures 2, 3, 5, and 6) to calculate $L_{\rm CE}$: $\kappa=10$ cm^2 g^{-1}, $\beta_{\rm m}=0.4$, $n=2$, and $\beta_0=0.05$. Note that this choice of parameters is for convenience and should not be regarded as unique for the central engine model.

In summary, with this central engine scenario, no additional KN components are required, and only a single red ejecta component is used. Here the new consideration is the additional thermal energy from the jet–ejecta interaction.

Figure 5 shows the bolometric light curve of our central-engine-powered model. In comparison to the r-process-powered blue KN model (see Figure 2), the central engine model light curve has a steeper decay. This fast evolution at early times is in contrast with the r-process model, as the issue of overpredicting the late red KN emission is avoided (see Section 3.1). This major difference is due to the thermal energy deposition at much earlier times relative to the diffusion timescale in the central engine model, whereas thermal energy is constantly being supplied to the system in the r-process model ($\propto t^{-1.3}$; see Section 2.1).

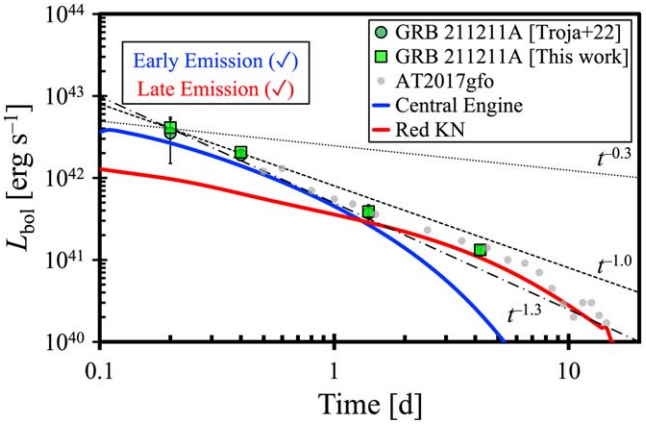

Figure 5. Same as Figure 2. The bolometric luminosity of our alternative central engine model, where a low-power jet launched by late engine activity interacts with the lanthanide-rich ejecta to explain the early (<1 day) KN emission in GRB 211211A (blue line), while the r-process explains the late (1 −4 days) red KN emission (red line) (see Figure 6 for the SED). This model can explain GRB 211211A data with only one red ejecta component. The parameters of the jet in the central engine model are jet isotropic equivalent luminosity $L_{\rm iso,0}=10^{47}$ erg s^{-1} and jet opening angle $\theta_0=7.^\circ5$.

Although the late low-power jet has in total an energy budget that is on the order of $\sim$a few percent[11] of that of the prompt jet, its blue KN-like emission is bright (e.g., compared to the prompt jet's cocoon; see Hamidani et al. 2024; also see Nakar & Piran 2017; Gottlieb et al. 2018; and the "shock-cooling" model in Arcavi 2018; Piro & Kollmeier 2018 for the prompt jet case). This is because (i) the system is expanding homologously and thermal energy is subjected to adiabatic cooling (as $\propto V^{-\frac{1}{3}}\propto t^{-1}$), and (ii) the blue KN peaks at $\sim$1 day $\sim10^5$ s. Therefore, by the peak time, ejecta heated by the prompt jet (launched at $\sim$1 s) would have cooled down adiabatically by a factor of $\sim10^{-5}$, whereas ejecta heated by the late jet (launched at $\sim10^4$ s) cool down only by a factor of $\sim10^{-1}$, which, combined with the low energy budget of the late jet, would still make the late jet model $\sim10-100$ times brighter than the prompt jet model.

In Figure 6, the SED of the central-engine-powered model is presented (double lines). The fast temporal evolution of the central engine model is noticeable (to be contrasted with r-process models in Figure 3). Combined with the r-process-powered red KN model, the central engine model is consistent with almost all data points at all epochs.

Besides naturally explaining the KN associated with GRB 211211A at all epochs, our central engine model is appealing in other aspects. First, it is consistent with the

[9] It should be noted that acceleration of ejecta shells due to energy supplied by the jet is assumed insignificant, as the kinetic energy of the ejecta dominates (see Hamidani & Ioka 2023b).

[10] Here we did not consider the possibility of disintegration of r-process heavy elements by the jet-cocoon shock (Horiuchi et al. 2012; Granot et al. 2023) because this would be inconsistent with observations of the late red KN.

[11] This can be found considering that the isotropic equivalent energy of the prompt emission of GRB 211211A is $\sim5\times10^{51}$ erg s^{-1} (Yang et al. 2022) and that the typical luminosity and duration of the average plateau phase gives an energy of $\sim10^{46}\times10^4\sim10^{50}$ erg (Kisaka et al. 2017). Radiation efficiencies were assumed to be comparable ($\eta_\gamma\sim10\%$; Matsumoto et al. 2020; Mei et al. 2022; Rouco Escorial et al. 2023; Hamidani et al. 2024).

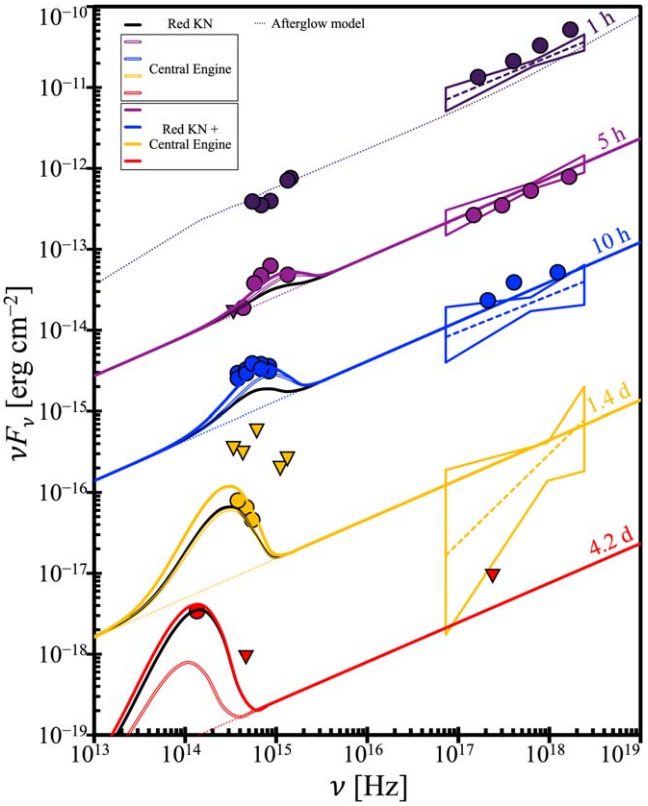

Figure 6. Same as Figure 3. The SED of our alternative central engine model, where a low-power jet launched by late engine activity interacts with the lanthanide-rich ejecta to explain the early (5−10 hr) blue KN emission in GRB 211211A (double lines), while the *r*-process explains the late (1.4−4.2 days) red KN emission (black line; same model as in Figures 2 and 3). The central engine model, combined with the red KN model (solid colored lines), can explain both early and late emission data (see Figure 5 for the bolometric luminosity).

detection of extended/plateau emission in SGRBs; this is also coherent with the detection of GeV emission in GRB 211211A and associated with the same type of jet (Mei et al. 2022). Hence, the consideration of a late jet is quite reasonable. In addition, the energy requirement for the late jet is just ∼a few percent of that of the prompt jet. This could naturally be explained by late-time accretion onto the merger remnant (e.g., Kisaka & Ioka 2015; Gottlieb et al. 2023; also, Lu & Quataert 2023 showed that this late jet is wider than the prompt jet).

Second, it only requires a single ejecta component. Here, this single ejecta component is red (i.e., lanthanide-rich; Waxman et al. 2018), which is consistent with numerical relatively calculations showing that the red dynamical ejecta is faster, shielding the bluer postmerger ejecta and giving the impression of an effectively red ejecta (Kawaguchi et al. 2018). There is no need to invoke a second blue (or even a third purple) component. In fact, they would typically require parameters that are not trivial considering numerical relativity calculation results (see Shibata et al. 2017; Fujibayashi et al. 2018; Siegel 2019), although other physical mechanisms have been suggested recently (e.g., Miller et al. 2019; Shibata et al. 2021; Just et al. 2023; also see Figure 9 in Kawaguchi et al. 2023).

The scenario of GRB central-engine-powered KNe has been proposed in Kisaka et al. (2015, 2016) in general terms (and in Ioka & Nakamura 2018 and Matsumoto et al. 2018 in the context of AT 2017gfo/GW170817). It has been suggested that the prompt jet can affect the color of the KN emission (bluer, Ciolfi & Kalinani 2020; Nativi et al. 2021; Combi & Siegel 2023; or redder, Shrestha et al. 2023). Troja et al. (2022) pointed out the possibility of the GRB jet's contribution to the KN associated with GRB 211211A. Meng et al. (2024) argued for the same from statistical fitting of Troja et al.'s (2022) results using a one-zone cocoon model. However, their model is not reasonable, as it assumes that the prompt jet somehow shocks most of the ejecta ($\sim 0.01\,M_\odot$) on a timescale of ∼1 s (inconsistent with numerical simulations; Murguia-Berthier et al. 2014; Nagakura et al. 2014; Gottlieb et al. 2018; Hamidani & Ioka 2021; etc.), depositing large amounts of thermal energy (also inconsistent with numerical simulations showing that kinetic energy dominates; see Figure 1 in Hamidani & Ioka 2021), which gives inappropriate luminosity and temperature estimates when compared with numerical simulation estimates (Gottlieb et al. 2018, 2023a) and realistic analytic modeling (in particular, see Section 4.3.2 in Hamidani & Ioka 2023b and Section 5.5 Hamidani & Ioka 2023a). Here, we demonstrate that energy injection from a long-lived central engine can naturally explain the KN associated with GRB 211211A, with the crucial difference being, instead of the prompt jet (Nakar & Piran 2017; Arcavi 2018; Piro & Kollmeier 2018; etc.), we suggest a late low-power plateau-like jet with a reasonable energy budget of ∼a few percent of the prompt jet's energy.

5. Discussion and Conclusion

Here, we revisited the early blue KN emission in GRB 211211A to better investigate its origin, having been previously explained using *r*-process heating.

We have presented a fully analytic KN model (Section 2.1) and explained that *r*-process-powered KNe follow a shallow temporal evolution at early times ($L_{\rm KN} \propto t^{-0.3}$) due to the continuous *r*-process energy deposition and the dominance of the diffusion of trapped thermal energy at early times (see Figure 1). We then applied our model to the KN emission associated with GRB 211211A (Section 2.2).

Our results indicate that the light curve of the early blue KN emission in GRB 211211A has a temporal evolution that is too fast to be explained via our analytic models (Section 3.1) in the parameter space: $M_{\rm e} \sim 0.01-0.05\,M_\odot$ (KN models with $M_{\rm e} < 0.01\,M_\odot$ or $M_{\rm e} > 0.05\,M_\odot$ are already excluded), $\kappa \sim 0.1-10$ cm^2 g^{-1}, $\beta_{\rm m} \sim 0.4-0.5$, and $n \sim 2-3.5$. The main issue is that the early data are too bright, and in order to explain this via the *r*-process-powered blue KN models, the required mass is large so that it leads to an overprediction of the red KN emission observed at late times, whereas the red KN model is too dim at early times to explain the early bright blue KN emission (see Figure 2). Employing low-opacity, low-mass blue KN models is not ideal either, as the resulting colors are too blue to be consistent with early data (see Figure 3). As a result, over our wide parameter space, we did not find any combination of two *r*-process-powered KN models (i.e., two components) that could explain the entire data set of GRB 211211A (see Figure 4).

We argue that the early data (5–10 hr) in GRB 211211A may not be predominantly *r*-process-powered. Our alternative is a central-engine-powered KN. We suggest that a low-power jet from late engine activity that interacts with the merger ejecta offers a more natural explanation, which is consistent with observations indicating that the majority of SGRBs have late,

long-lasting extended/plateau emission phases after the prompt emission (Kisaka et al. 2017). Also, GeV emission observed $\sim 10^4$ s after GRB 211211A has been explained with the same type of engine activity, jet, and timescale (Mei et al. 2022). We showed that such a low-power jet ($\sim 10^{46}$ erg s^{-1} in X-ray) with its typical opening angle ($\sim 7.^{\circ}5$) naturally explains the bolometric light curve (see Figure 5) and the SED at all epochs (see Figure 6).

Hence, our conclusion is that the early blue KN emission in GRB 211211A hints at late engine activity. This suggests that after the prompt emission, a late low-power engine activity phase may be quite common in SGRBs and also potentially in LGRBs (as X-ray flares; Nousek et al. 2006). We argue that the interaction of this late jet with the surrounding ejecta could not have been identified in most standard/cosmological GRBs due to its faintness at large distances. In the multimessenger event GW170817/AT 2017gfo, the first observations started at ∼10 hr; hence, any early blue emission has been missed. However, GRB 211211A as a nearby, well-observed event may have opened a new window to indirectly probe the evolution of the central engine of GRBs at later times after the prompt phase. Rossi et al. (2020) suggested that several KN candidates associated with SGRBs show exceptionally bright blue KNe (e.g., GRB 050724, GRB 060614, and GRB 070714B), while their red KNe are typical; this is challenging to explain with *r*-process heating but can be explained naturally with our scenario of a late low-power jet.

Our result shows that a typical late low-power jet model ($\sim 10^{46}$ erg s^{-1} in X-ray and $\sim 7.^{\circ}5$) synergizes well with the red ejecta component to explain the blue KN. However, it should be noted that alternative jet models may be viable. Different central-engine-powered models such as the magnetar model have not been investigated here (Yu et al. 2013; Metzger et al. 2018). However, high neutrino radiation from the deferentially rotating hypermassive NS remnant can be a potential issue, as neutrinos increase the electron fraction (Y_e) of the ejecta and suppress nucleosynthesis of heavy elements, which would be at odds with the red KN emission (Metzger & Fernández 2014).[12] Additionally, the magnetar model could face the issue of producing a KN that is too bright when compared to the observations (Wang et al. 2024), and even if the magnetar outflow is collimated and on-axis (Wang et al. 2024), GRB 211211A would be expected to have a much brighter KN. Finally, the magnetar model may not have as coherent an explanation for the GeV emission in GRB 211211A as our low-power jet model (Mei et al. 2022).

Our main finding here is that the current *r*-process-powered blue KN models struggle at explaining the observed emission after GRB 211211A. Here, we used a simplified model of the heating rate ($\propto t^{-1.3}$); however, it should be stressed that *r*-process models are still incomplete and uncertain (Barnes et al. 2021; Zhu et al. 2021; Mumpower et al. 2024).[13] For instance, the heating rate could have a steeper decay for some very specific models (with high Y_e; see Figure 5 in Wanajo et al. 2014). Although such models are not typical, they could present an alternative explanation for the KN emission following GRB 211211A. It should be stressed that we do not rule out the existence of the *r*-process-powered blue KN or the existence of a blue (or purple) ejecta component. Instead, we indicate that it is subdominant in luminosity and cannot fully explain the observed early emission. Hence, it could still coexist with the engine-powered emission in our scenario.

It should also be noted that in terms of radiative transfer, our result relied on two simplifications: gray opacity (although the adopted values are compatible with realistic radioactive transfer simulations; Banerjee et al. 2024) and a single-temperature blackbody model. In reality, radiative transfer in the KN ejecta can be more complex, which could result in a more fluctuating light curve (although at short timescales; see Banerjee et al. 2024) and reprocessing of radiation.

Also, we explored a wide parameter space (in particular for κ and M_e) that, with the current understanding, is expected to cover a typical BNS event; however, considering the diversity in BNS and BH–NS mergers, extreme parameters that we did not cover could be possible in nature (e.g., see Kawaguchi et al. 2024).

Finally, despite the KN of GRB 211211A being nearby and well observed, there are gaps in the observations (in particular the SED) and systematic uncertainties, especially considering the uncertainties in afterglow modeling (Lamb et al. 2022). Hence, although we disfavor the current *r*-process model for the current data set of GRB 211211A, more research (e.g., nuclear physics and *r*-process nucleosynthesis) and more observations are needed to reach a more general conclusion on SGRBs.

With more GRB-related missions available, such as the Einstein Probe (Yuan et al. 2015) and SVOM (Cordier et al. 2015) and, in the near future, ULTRASAT (Shvartzvald et al. 2024), HiZ-GUNDAM (Yonetoku et al. 2020), THESEUS (Amati et al. 2018), etc., the prospect of more and very early observations/follow-ups of GRBs, BNS/BH–NS mergers, and X-ray transients is promising. Our proposed scenario of engine-powered early KNe can be tested with such future observations, together with the scenario of *r*-process-powered KN. Also, our scenario of late engine activity is very relevant to neutrino emission and could be tested with future neutrino observations (Matsui et al. 2024).

Acknowledgments

We thank Alessio Mei, Ayari Kitamura, Clément Pellouin, Kazumi Kashiyama, Kunihito Ioka, Nanae Domoto, Norita Kawanaka, Om S. Salafia, Sho Fujibayashi, Smaranika Banerjee, Tomoki Wada, and Wataru Ishizaki for the fruitful discussions and comments.

This research was supported by the Japan Science and Technology Agency (JST) FOREST Program (grant No. JPMJFR212Y), the Japan Society for the Promotion of Science (JSPS) Grant-in-Aid for Scientific Research (19H00694, 20H00158, 20H00179, 21H04997, 23H00127, 23H04894, 23H04891, 23H05432, and 23K19059), JSPS Bilateral Joint Research Project, and National Institute for Fusion Science (NIFS) Collaborative Research Program (NIFS22KIIF005).

This work was partly supported by JSPS KAKENHI Nos. 22K14028, 21H04487, and 23H04899 (S.S.K.). S.S.K. acknowledges the support by the Tohoku Initiative for Fostering Global Researchers for Interdisciplinary Sciences

[12] It should be noted that recent works indicate that even in cases where the remnant is a BH, the disk outflow tends to have a higher Y_e (see Fujibayashi et al. 2020; Just et al. 2022); hence, the formation mechanism of high-opacity massive ejecta is still being investigated, although MHD effects may favor lower Y_e values (Kiuchi et al. 2023).

[13] Is it worth noting that with revised heating rates, Sarin & Rosswog (2024) found that the decline rates of KNe are typically overestimated (i.e., they decline more slowly than classically considered with simple models). This further supports our conclusion.

(TI-FRIS) of MEXT's Strategic Professional Development Program for Young Researchers. G.P.L. is supported by the Royal Society via a Dorothy Hodgkin Fellowship (grant Nos. DHF-R1-221175 and DHF-ERE-221005).

Numerical computations were achieved thanks to the following: the Cray XC50 of the Center for Computational Astrophysics at the National Astronomical Observatory of Japan and the Cray XC40 at the Yukawa Institute Computer Facility.

Data Availability

The data underlying this Letter will be shared on reasonable request to the corresponding author.

Appendix
Data of the KN in GRB 211211A

GRB 211211A's photometric infrared/optical/UV data are gathered from the literature (Rastinejad et al. 2022; Troja et al. 2022). Similarly to Troja et al. (2022), we consider five epochs as a function of the observed time (since the GRB): 1 hr, 5 hr, 10 hr, 1.4 days, and 4.2 days.

X-ray data are obtained from Swift's Burst Analyser webpage.[14] X-ray data are integrated over the intervals 3.5×10^3–5×10^3 s, 15.9×10^3–22.1×10^3 s, 20.0×10^3–64.8×10^3 s, and 50.0×10^3 –300.0×10^3 s, so that the logarithmic central times correspond to the times of each respective epoch (all epochs except 4.2 days). For each epoch, we determine the photon index (Γ) and the normalization level. Considering uncertainties in both parameters, X-ray observations are represented in the form of bow ties (see Figures 3 and 6).

In addition, X-ray data points in Troja et al. (2022) are used as a reference; except for the 1.4 day epoch (where the photon arrival time is not well consistent with the epoch time), all epochs are considered.

A.1. Afterglow Model

Rastinejad et al. (2022), using a Markov Chain Monte Carlo, fit a decelerating, relativistic forward shock with synchrotron emission model (see Lamb et al. 2018) to the afterglow-dominated data from GRB 211211A. The fit model parameters are determined via the X-ray and radio afterglow data, with the early optical/near-infrared (NIR) providing an SED constraint to the model and the later (>0.1 day) KN-dominated optical/NIR data providing upper limits for the afterglow model. This light-curve fit allows for the subtraction of the afterglow contribution to the KN-dominated optical/NIR data. The optical afterglow emission at >0.1 day is within the self-similar deceleration phase and behaves as a simple power-law decline governed by the spectral and temporal indices inferred from the X-ray to radio broadband data.

The afterglow model assumes a uniform "top-hat" jet structure viewed on-axis, where the bright GRB 211211A supports the "on-axis viewer" assumption. The observable afterglow emission from a jet with an ultrarelativistic velocity, where the Lorentz factor is ∼70 (Rastinejad et al. 2022), is emitted from within a narrow cone with an angle defined by the inverse of the Lorentz factor, initially <1°. Any wide-angle jet structure will be hidden to an on-axis observer until the jet break time, when, as the jet decelerates, the inverse of the Lorentz factor becomes comparable to the jet core half-opening angle. At the jet break time, the afterglow decline will typically steepen, and the shape of the jet break (how sharp/rapid the jet break is) contains information about the extent of any wider-angled jet structure (Lamb et al. 2021). Observations rarely have sufficient cadence and sensitivity at the jet break time to accurately determine the sharpness of the light-curve change; thus, the top-hat jet structure assumption is a valid approximation for most bright, and therefore on-axis-viewed, GRBs.

The SEDs of our afterglow model have been compared to the X-ray data. Apart from epoch 4 (1.4 days), where the X-rays became too faint, our fit is consistent with the measured X-ray photon index. Our afterglow model is also consistent with IR/optical/UV data (see dotted lines in Figure 3).

Our afterglow modeling confirms the presence of the thermal excess previously reported by Rastinejad et al. (2022) and Troja et al. (2022) (see Appendix A.2). We assessed the effect of uncertainties in the afterglow modeling on the flux of the thermal excess and confirmed that, within 1σ errors, their impact on the thermal excess is negligible (less than 10%). Thus, this afterglow model, with the previously mentioned reasonable assumptions, robustly predicts the presence of a thermal component.

A.2. Bolometric Luminosity

After subtracting the afterglow contribution, excess in IR/optical/UV that is interpreted as KN emission is found. Assuming a blackbody emission model, we determine the best fit (temperature and photospheric radius) for the excess. Our results are shown in Table 1 in comparison to those of Troja et al. (2022). Our fit is very consistent with Troja et al. (2022), despite differences in afterglow modeling. It should be noted that, due to

Table 1
Parameters of the Best Fit for the Afterglow Excess in GRB 211211A, in Comparison to Fitting Results in Troja et al. (2022)

Time (days)	Our Fit			Troja+22		
	$L_{\rm bol}$ (10^{42} erg s^{-1})	T (10^3 K)	$r_{\rm ph}$ (10^{15} cm)	$L_{\rm bol}$ (10^{42} erg s^{-1})	T (10^3 K)	$r_{\rm ph}$ (10^{15} cm)
0.2	4.11 ± 1.07	14.55 ± 3.32	0.36 ± 0.13	3.50 ± 2.00	16.00 ± 5.00	0.28 ± 0.14
0.4	2.05 ± 0.06	8.04 ± 0.28	0.83 ± 0.056	1.90 ± 0.15	8.00 ± 0.30	0.80 ± 0.05
1.4	0.39 ± 0.04	3.98 ± 0.18	1.47 ± 0.21	0.37 ± 0.10	4.90 ± 0.50	0.90 ± 0.20
4.2	0.13	2.68	1.90	0.13 ± 0.02	2.50 ± 0.10	2.00 ± 0.20

Note. 1σ errors are given. Errors in the 4.2 day epoch could not be statistically evaluated due to the limited data (only two data points).

[14] https://www.swift.ac.uk/burst_analyser/01088940/

the limited spectral coverage (in particular in UV at later epochs), this bolometric luminosity should be considered as a lower limit for the KN emission in the form of afterglow excess.

It should also be noted that, as our fit is statistical, the fitting results (photospheric radius in particular) do not necessarily have a robust physical meaning. For instance, in our physical model (that could explain the data), the maximum physical photospheric velocity $\beta_{\rm ph}$ is <0.4, while the fitting results indicate photospheric velocities $\beta_{\rm ph} > 0.4$ at early times. Hence, these photospheric values should not be taken at face value for their physical meaning.

ORCID iDs

Hamid Hamidani https://orcid.org/0000-0003-2866-4522
Masaomi Tanaka https://orcid.org/0000-0001-8253-6850
Shigeo S. Kimura https://orcid.org/0000-0003-2579-7266
Gavin P. Lamb https://orcid.org/0000-0001-5169-4143
Kyohei Kawaguchi https://orcid.org/0000-0003-4443-6984

References

Abbott, B. P., Abbott, R., Abbott, T. D., et al. 2017a, PhRvL, 119, 161101
Abbott, B. P., Abbott, R., Abbott, T. D., et al. 2017b, ApJL, 848, L13
Acciari, V. A., Ansoldi, S., Antonelli, L. A., et al. 2021, ApJ, 908, 90
Amati, L., O'Brien, P., Götz, D., et al. 2018, AdSpR, 62, 191
Arcavi, I. 2018, ApJL, 855, L23
Arnett, W. D. 1982, ApJ, 253, 785
Banerjee, S., Tanaka, M., Kato, D., & Gaigalas, G. 2024, ApJ, 968, 64
Barnes, J., Kasen, D., Wu, M.-R., & Martínez-Pinedo, G. 2016, ApJ, 829, 110
Barnes, J., Zhu, Y. L., Lund, K. A., et al. 2021, ApJ, 918, 44
Barthelmy, S. D., Cannizzo, J. K., Gehrels, N., et al. 2005a, ApJL, 635, L133
Barthelmy, S. D., Chincarini, G., Burrows, D. N., et al. 2005b, Natur, 438, 994
Burrows, D. N., Romano, P., Falcone, A., et al. 2005, Sci, 309, 1833
Ciolfi, R., & Kalinani, J. V. 2020, ApJL, 900, L35
Combi, L., & Siegel, D. M. 2023, PhRvL, 131, 231402
Cordier, B., Wei, J., Atteia, J. L., et al. 2015, arXiv:1512.03323
Drout, M. R., Piro, A. L., Shappee, B. J., et al. 2017, Sci, 358, 1570
Evans, P. A., Cenko, S. B., Kennea, J. A., et al. 2017, Sci, 358, 1565
Fong, W., Berger, E., & Fox, D. B. 2010, ApJ, 708, 9
Fong, W.-f., Nugent, A. E., Dong, Y., et al. 2022, ApJ, 940, 56
Fujibayashi, S., Kiuchi, K., Nishimura, N., Sekiguchi, Y., & Shibata, M. 2018, ApJ, 860, 64
Fujibayashi, S., Shibata, M., Wanajo, S., et al. 2020, PhRvD, 101, 083029
Gao, H., Lei, W.-H., & Zhu, Z.-P. 2022, ApJL, 934, L12
Gillanders, J. H., Troja, E., Fryer, C. L., et al. 2023, arXiv:2308.00633
Gompertz, B. P., O'Brien, P. T., Wynn, G. A., & Rowlinson, A. 2013, MNRAS, 431, 1745
Goodman, J. 1986, ApJL, 308, L47
Gottlieb, O., Issa, D., Jacquemin-Ide, J., et al. 2023a, ApJL, 953, L11
Gottlieb, O., Metzger, B. D., Quataert, E., et al. 2023b, ApJL, 958, L33
Gottlieb, O., Nakar, E., & Piran, T. 2018, MNRAS, 473, 576
Granot, A., Levinson, A., & Nakar, E. 2023, arXiv:2305.08575
Gupta, R., Pandey, S. B., Ror, A., et al. 2021, GCN, 31299, 1
Hamidani, H., & Ioka, K. 2021, MNRAS, 500, 627
Hamidani, H., & Ioka, K. 2023a, MNRAS, 524, 4841
Hamidani, H., & Ioka, K. 2023b, MNRAS, 520, 1111
Hamidani, H., Kimura, S. S., Tanaka, M., & Ioka, K. 2024, ApJ, 963, 137
Hamidani, H., Kiuchi, K., & Ioka, K. 2020, MNRAS, 491, 3192
Horiuchi, S., Murase, K., Ioka, K., & Mészáros, P. 2012, ApJ, 753, 69
Hotokezaka, K., & Nakar, E. 2020, ApJ, 891, 152
Hotokezaka, K., Wanajo, S., Tanaka, M., et al. 2016, MNRAS, 459, 35
Ioka, K., Kobayashi, S., & Zhang, B. 2005, ApJ, 631, 429
Ioka, K., & Nakamura, T. 2018, PTEP, 2018, 043E02
Ishizaki, W., Kiuchi, K., Ioka, K., & Wanajo, S. 2021, ApJ, 922, 185
Iwamoto, K., Mazzali, P. A., Nomoto, K., et al. 1998, Natur, 395, 672
Just, O., Goriely, S., Janka, H. T., Nagataki, S., & Bauswein, A. 2022, MNRAS, 509, 1377
Just, O., Vijayan, V., Xiong, Z., et al. 2023, ApJL, 951, L12
Kagawa, Y., Yonetoku, D., Sawano, T., et al. 2019, ApJ, 877, 147
Kasen, D., & Barnes, J. 2019, ApJ, 876, 128
Kasliwal, M. M., Nakar, E., Singer, L. P., et al. 2017, Sci, 358, 1559
Kawaguchi, K., Domoto, N., Fujibayashi, S., et al. 2024, arXiv:2404.15027
Kawaguchi, K., Fujibayashi, S., Domoto, N., et al. 2023, MNRAS, 525, 3384
Kawaguchi, K., Shibata, M., & Tanaka, M. 2018, ApJL, 865, L21
Kimura, S. S., Murase, K., Ioka, K., et al. 2019, ApJL, 887, L16
Kisaka, S., & Ioka, K. 2015, ApJL, 804, L16
Kisaka, S., Ioka, K., & Nakar, E. 2016, ApJ, 818, 104
Kisaka, S., Ioka, K., & Sakamoto, T. 2017, ApJ, 846, 142
Kisaka, S., Ioka, K., & Takami, H. 2015, ApJ, 802, 119
Kiuchi, K., Fujibayashi, S., Hayashi, K., et al. 2023, PhRvL, 131, 011401
Kouveliotou, C., Meegan, C. A., Fishman, G. J., et al. 1993, ApJL, 413, L101
Kulkarni, S. R. 2005, arXiv:astro-ph/0510256
Lamb, G. P., Kann, D. A., Fernández, J. J., et al. 2021, MNRAS, 506, 4163
Lamb, G. P., Mandel, I., & Resmi, L. 2018, MNRAS, 481, 2581
Lamb, G. P., Nativi, L., Rosswog, S., et al. 2022, Univ, 8, 612
Lamb, G. P., Tanvir, N. R., Levan, A. J., et al. 2019, ApJ, 883, 48
Levan, A. J., Gompertz, B. P., Salafia, O. S., et al. 2024, Natur, 626, 737
Li, L.-X., & Paczyński, B. 1998, ApJL, 507, L59
Lu, W., & Quataert, E. 2023, MNRAS, 522, 5848
MacFadyen, A. I., & Woosley, S. E. 1999, ApJ, 524, 262
Matsui, R., Kimura, S. S., & Hamidani, H. 2024, arXiv:2405.07695
Matsumoto, T., Ioka, K., Kisaka, S., & Nakar, E. 2018, ApJ, 861, 55
Matsumoto, T., Kimura, S. S., Murase, K., & Mészáros, P. 2020, MNRAS, 493, 783
Mei, A., Banerjee, B., Oganesyan, G., et al. 2022, Natur, 612, 236
Meng, Y.-Z., Wang, X. I., & Liu, Z.-K. 2024, ApJ, 963, 112
Metzger, B. D., & Fernández, R. 2014, MNRAS, 441, 3444
Metzger, B. D., Martínez-Pinedo, G., Darbha, S., et al. 2010, MNRAS, 406, 2650
Metzger, B. D., Thompson, T. A., & Quataert, E. 2018, ApJ, 856, 101
Miller, J. M., Ryan, B. R., Dolence, J. C., et al. 2019, PhRvD, 100, 023008
Mumpower, M. R., Sprouse, T. M., Miller, J. M., et al. 2024, ApJ, 970, 173
Murguia-Berthier, A., Montes, G., Ramirez-Ruiz, E., De Colle, F., & Lee, W. H. 2014, ApJL, 788, L8
Nagakura, H., Hotokezaka, K., Sekiguchi, Y., Shibata, M., & Ioka, K. 2014, ApJL, 784, L28
Nakar, E., & Piran, T. 2017, ApJ, 834, 28
Nakar, E., & Sari, R. 2012, ApJ, 747, 88
Nativi, L., Bulla, M., Rosswog, S., et al. 2021, MNRAS, 500, 1772
Norris, J. P., & Bonnell, J. T. 2006, ApJ, 643, 266
Nousek, J. A., Kouveliotou, C., Grupe, D., et al. 2006, ApJ, 642, 389
Nugent, A. E., Fong, W.-F., Dong, Y., et al. 2022, ApJ, 940, 57
O'Connor, B., Troja, E., Dichiara, S., et al. 2022, MNRAS, 515, 4890
Paczynski, B. 1986, ApJL, 308, L43
Piro, A. L., & Kollmeier, J. A. 2018, ApJ, 855, 103
Rastinejad, J. C., Gompertz, B. P., Levan, A. J., et al. 2022, Natur, 612, 223
Rossi, A., Stratta, G., Maiorano, E., et al. 2020, MNRAS, 493, 3379
Rosswog, S., Feindt, U., Korobkin, O., et al. 2017, CQGra, 34, 104001
Rouco Escorial, A., Fong, W., Berger, E., et al. 2023, ApJ, 959, 13
Sarin, N., & Rosswog, S. 2024, arXiv:2404.07271
Shibata, M., Fujibayashi, S., Hotokezaka, K., et al. 2017, PhRvD, 96, 123012
Shibata, M., Fujibayashi, S., & Sekiguchi, Y. 2021, PhRvD, 104, 063026
Shrestha, M., Bulla, M., Nativi, L., et al. 2023, MNRAS, 523, 2990
Shvartzvald, Y., Waxman, E., Gal-Yam, A., et al. 2024, ApJ, 964, 74
Siegel, D. M. 2019, EPJA, 55, 203
Stanek, K. Z., Matheson, T., Garnavich, P. M., et al. 2003, ApJL, 591, L17
Tanaka, M., Utsumi, Y., Mazzali, P. A., et al. 2017, PASJ, 69, 102
Troja, E., Fryer, C. L., O'Connor, B., et al. 2022, Natur, 612, 228
Veres, P., Bhat, P. N., Burns, E., et al. 2023, ApJL, 954, L5
Villar, V. A., Guillochon, J., Berger, E., et al. 2017, ApJL, 851, L21
Wanajo, S., Sekiguchi, Y., Nishimura, N., et al. 2014, ApJL, 789, L39
Wang, H., Beniamini, P., & Giannios, D. 2024a, MNRAS, 527, 5166
Wang, Y., Zhang, B., & Zhu, Z. 2024b, MNRAS, 528, 3705
Waxman, E., Ofek, E. O., Kushnir, D., & Gal-Yam, A. 2018, MNRAS, 481, 3423
Waxman, E., Ofek, E. O., & Kushnir, D. 2019, ApJ, 878, 93
Yang, J., Ai, S., Zhang, B.-B., et al. 2022, Natur, 612, 232
Yang, Y.-H., Troja, E., O'Connor, B., et al. 2024, Natur, 626, 742
Yonetoku, D., Mihara, T., Doi, A., et al. 2020, Proc. SPIE, 11444, 114442Z
Yu, Y.-W., Zhang, B., & Gao, H. 2013, ApJL, 776, L40
Yuan, W., Zhang, C., Feng, H., et al. 2015, arXiv:1506.07735
Zhang, B. T., Murase, K., Yuan, C., Kimura, S. S., & Mészáros, P. 2021, ApJL, 908, L36
Zhang, H.-M., Huang, Y.-Y., Zheng, J.-H., Liu, R.-Y., & Wang, X.-Y. 2022, ApJL, 933, L22
Zhu, Y. L., Lund, K. A., Barnes, J., et al. 2021, ApJ, 906, 94